Characterization of the I_2^- anion ground state using conventional and femtosecond photoelectron spectroscopy

Martin T. Zanni, Travis R. Taylor, B. Jefferys Greenblatt, Benoit Soep,[a)]
and Daniel M. Neumark
Department of Chemistry, University of California, Berkeley, California and Chemical Sciences Division, Lawrence Berkeley National Laboratory, Berkeley, California

(Received 11 July 1997; accepted 14 August 1997)

The $\tilde{X}\ ^2\Sigma_u^+$ state of the I_2^- anion has been fit to a Morse potential using data from two techniques: conventional and femtosecond photoelectron spectroscopy (FPES). Conventional photoelectron spectroscopy is used to determine the adiabatic electron affinity of I_2 as well as the well depth and equilibrium nuclear geometry of I_2^-. In the FPES experiment, the pump pulse induces coherent nuclear motion on the ground state of I_2^- by resonant impulsive stimulated Raman scattering (RISRS), and the vibrational frequency of the anion is determined from the resulting oscillatory structure in the time-dependent photoelectron spectra. We find the electron affinity (EA) of I_2 to be 2.524 ± 0.005 eV, the well depth (D_e) for I_2^- to be 1.014 ± 0.005 eV, the equilibrium internuclear separation (R_e) to be 3.205 ± 0.005 Å, and the vibrational frequency to be $110 \pm 2\ cm^{-1}$. These values for the I_2^- potential parameters differ significantly from previous results. © *1997 American Institute of Physics.* [S0021-9606(97)02743-8]

I. INTRODUCTION

In recent years, the role of solute/solvent interactions on chemical dynamics has been explored in experiments that probe the photodissociation of anions in liquids and size-selected clusters. The I_2^- anion has been a particularly attractive target for this type of investigation; its photodissociation dynamics have been studied in size-selected $I_2^-(CO_2)_n$[1–3] and $I_2^-(Ar)_n$[3,4] clusters and in several polar solvents.[5–7] The interpretation of these experiments relies at least in part on the potential energy curves for the ground and low-lying excited states of I_2^-, but the potential energy curves available in the literature are at best approximately correct. In this study we have constructed an improved potential for the ground state of I_2^- using a combination of conventional (~ 10 meV resolution) and femtosecond photoelectron spectroscopy. As part of this study, we have demonstrated a new method for determining vibrational frequencies in gas phase negative ions using femtosecond photoelectron spectroscopy.

The most widely referenced potential curves for the I_2^- ground and excited states are the Morse potentials constructed by Chen and Wentworth,[8] of which the ground and second excited states are shown in Fig. 1. These are based on an assortment of experimental data including Raman spectroscopy in matrices, electronic spectroscopy in crystals, and gas-phase dissociative attachment experiments. However, there remains a large degree of uncertainty in these semiempirical curves as each is constructed from, at most, four experimental parameters. In addition, the parameters taken from matrices and crystals are likely to be perturbed from the gas phase values. Recently, Chen and co-workers[9] published new potentials for I_2^- in which the equilibrium internuclear distance of the ground state was taken to be the sum of the ionic and covalent radii of I^- and I, respectively. This resulted in a significant increase in the bond length, from 3.23 to 3.385 Å and a decrease in the well depth from 1.10 to 1.055 eV, with even larger changes in the excited states. In the most recent paper from this group,[10] the proposed equilibrium bond length was further increased by 0.015 Å and the well depth was again increased by 0.051 eV, based on correlations with the Morse parameters for the isoelectronic rare gas positive ion, Xe_2^+. The parameters for the three potentials are listed in Table I.

The I_2^- electronic states have also been investigated by *ab initio* methods, but these studies are complicated by the large number of electrons and strong spin–orbit coupling. The few calculations performed have been limited to valence bond methods by Tasker *et al.*,[11] self-consistent field (SCF) calculations by Bowmaker *et al.*,[12] and relativistic core potential calculations by Shaik and co-workers.[13] Maslen *et al.*,[14] using a multireference configuration interaction (MRCI) calculation for the ground and excited states, have recently incorporated spin–orbit effects for the first time. Compared to the three semiempirical potentials proposed by Chen and co-workers, Maslen *et al.* predict a shallower anion ground state potential, 0.905 eV, and a bond length of 3.33 Å that lies between the various values proposed by Chen and co-workers.[8–10] The considerable variation in the potential parameters for I_2^-, particularly the bond length, is in stark contrast to the precisely known neutral state curves, generated using the RKR inversion technique with vibrational energies and rotational constants derived from fluorescence data.[15–18]

In this paper, we use a combination of conventional and femtosecond photoelectron spectroscopy (FPES) techniques to characterize the I_2^- ground state. The conventional photoelectron spectrum obtained at 10 meV resolution yields vibrationally resolved bands representing transitions from I_2^- to

[a)]Visiting Miller Professor. Permanent address: Laboratoire de Photophysique Moléculaire, Université Paris-Sud, Orsay 91405, France.

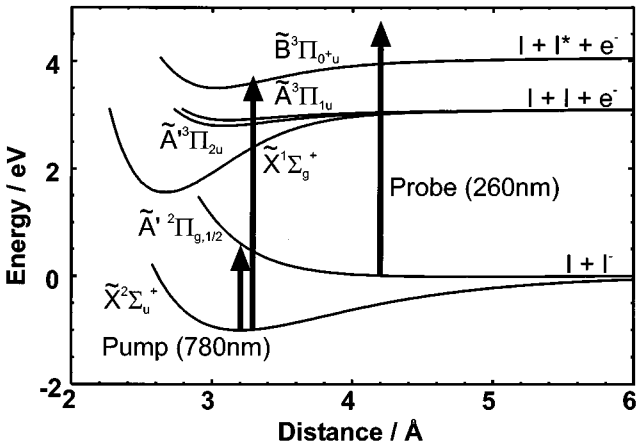

FIG. 1. Potential energy curves for the relevant electronic states of I_2^- and I_2 taken from Refs. 15–18. The pump and probe wavelengths are shown for the FPES experiment, probing the ground and excited state potentials.

the $\tilde{X}\ ^1\Sigma_g^+$, $\tilde{A}'\ ^3\Pi_{2u}$, and $\tilde{A}\ ^3\Pi_{1u}$ states of I_2. Because the three I_2 electronic states are well characterized, our photoelectron spectrum yields an accurate adiabatic electron affinity of I_2. In addition, we determine the I_2^- well depth, equilibrium internuclear separation, and vibrational temperature.

Anion FPES is a relatively new femtosecond pump–probe technique which we have used recently to investigate the excited state dynamics of both I_2^- and $I_2^-Ar_n$ clusters.[4,19] In this experiment, I_2^- is excited to the $\tilde{A}'\ ^2\Pi_{1/2,g}$ state by a femtosecond pump pulse, and the photoelectron spectrum of the evolving system is measured at a series of delay times by photodetachment with a second femtosecond probe pulse. Here we demonstrate that the pump pulse induces vibrational coherences on the I_2^- ground state that can be readily detected as oscillatory structure in the time-dependent photoelectron spectra. The process by which the coherences are induced as analogous to that seen in condensed phase studies of I_3^- by Ruhman and co-workers.[20] We obtain the gas phase I_2^- vibrational frequency from the oscillations in our spectra. This frequency along with the information obtained from the conventional photoelectron spectrum leads to a much-improved potential for the I_2^- ground state.

II. EXPERIMENT

The conventional and femtosecond photoelectron spectroscopy experiments are carried out on two different time-of-flight photoelectron spectrometers. Each has been described previously,[19,21,22] but a brief summary will be given here and the differences between the instruments outlined.

In both experiments, argon carrier gas (15 psig) is passed over crystalline I_2 and supersonically expanded through a pulsed piezo electric valve.[23] Anions are generated by a 1 keV electron beam which crosses the expansion just downstream of the nozzle, and are injected into a Wiley–McLaren time-of-flight mass spectrometer[24] by applying pulsed extraction and acceleration fields perpendicular to the molecular beam axis. An additional reflectron stage in the conventional photoelectron spectrometer provides higher mass resolution, although this is not needed for the work presented here. After passing through several differentially pumped regions, the ions enter the detector chamber where they interact with one or more laser pulses. An in-line microchannel plate detector is used to monitor the ion beam.

In the conventional spectrometer, the ions are photodetached with a pulsed Nd:YAG laser operating at a repetition rate of 20 Hz. The photodetachment photon energy of 4.141 eV (299 nm) is obtained by Raman-shifting the fourth harmonic (266 nm) of the Nd:YAG fundamental in high pressure H_2. The electron kinetic energies are measured by time-of-flight through a 100 cm long field-free region. The instrumental resolution is 8–10 meV for an electron kinetic energy (eKE) of 0.65 eV and degrades as $(eKE)^{3/2}$.

The femtosecond photoelectron spectrometer has been optimized to be compatible with the high laser repetition rate, 500 Hz in these experiments, and the low photoelectron signal expected for a two-photon pump-and-probe experiment. The pulsed piezoelectric valve operates at the laser repetition rate, and the resulting large gas load is handled with two diffusion pumps totaling 8800 ℓ/s of pumping speed on the ion source chamber. In addition, a ''magnetic bottle'' time-of-flight analyzer[25] is used to yield a considerably higher photoelectron collection efficiency, $>50\%$ vs $<0.1\%$ for the field-free design. In the work reported here, the resolution of the femtosecond spectrometer is approximately 200 meV for 1 eV electrons.

The FPES experiment uses a commercial laser system to

TABLE I. Spectroscopic constants for the ground state of I_2^-.

	Current work	*Ab initio*[a]	Chen & Wentworth[b]	Dojahn *et al.*[c]	Chen *et al.*[d]
R_e (Å)	3.205±0.005	3.33	3.23	3.385	3.40
D_e (eV)	1.014±0.005	0.905	1.10	1.055	1.106[e]
ω_e (cm^{-1})	110±2	99.9	113	115	116

[a]Reference 14.
[b]Reference 8.
[c]Reference 9.
[d]Reference 10.
[e]Reported value is $D_0 = 1.099$ eV. D_e determined by adding 0.007 eV zero point energy.

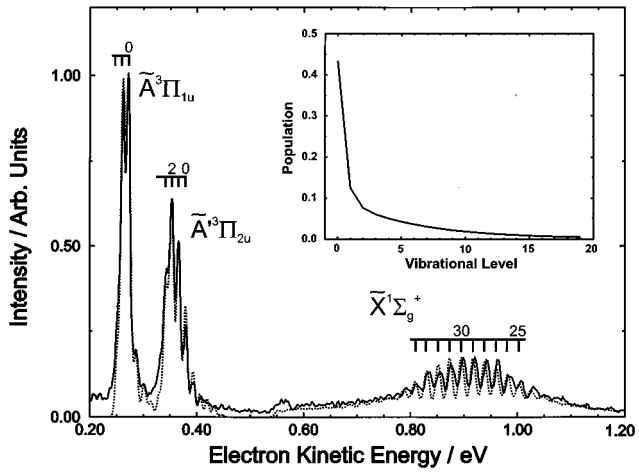

FIG. 2. Conventional photoelectron spectrum taken at 299 nm. Experimental spectrum is shown solid and simulations dashed. Transitions to neutral electronic states are labeled and vibrational progressions marked for transitions from $v=0$ of the anion. The inset shows the anion vibrational population used in the simulation.

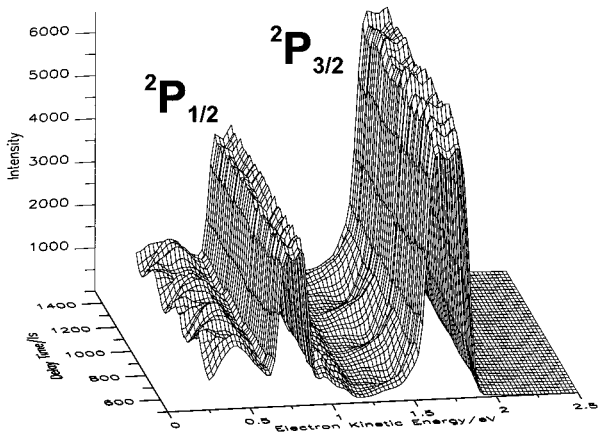

FIG. 3. Experimental FPES spectra of I_2^-. Spectra at delay times ranging from 500 to 1500 fs in 25 fs steps. Assignments of atomic iodine features are indicated.

generate the femtosecond pump and probe pulses. A Coherent Innova-90 Ar^+ laser pumps a Clark-MXR NJA-5 Ti:Sapphire oscillator. Selected pulses are amplified using a Clark-MXR regenerative amplifier that includes a pulse stretcher, Ti:Sapphire regenerative amplifier pumped by a Nd:YAG laser running at a repetition rate of 500 Hz, and a pulse compressor. At 780 nm the resulting pulse widths and energies were 75 fs at FWHM (sech^2) and 1 mJ, respectively. Seventy percent of this beam is split and tripled, resulting in a probe pulse at 260 nm, 105 fs wide and with 20 μJ of energy, characterized by difference frequency cross correlation in a 200 μm thick KDP crystal. The remaining 30% of the 780 nm pulse passes through a computer controlled delay line and acts as the pump pulse.

III. RESULTS

A. Conventional photoelectron spectrum

The photoelectron spectra of I_2^- at $h\nu=4.141$ eV is presented in Fig. 2. This spectrum was taken with the laser polarized at 54.7° with respect to the direction of electron detection (the ''magic'' angle), and is plotted as a function of electron kinetic energy (eKE). The eKE is related to the internal energy of the neutral molecule by the expression

$$\mathrm{eKE}=h\nu-\mathrm{EA}-(T_0+E_v^0)+E_v^-, \tag{1}$$

where $h\nu$ is the photon energy and EA is the adiabatic electron affinity corresponding to the difference in energy between the lowest vibrational state of the anion to the lowest vibrational state of the neutral. E_v^0 and E_v^- are the vibrational energies above the zero point energy of the anion and neutral, respectively, and T_0 is the term value for the electronic state of the neutral. A simulated spectrum (dashed line) is superimposed on the experimental spectrum and discussed in Sec. IV B.

The spectrum shows three bands corresponding to transitions from the anion ground state to the lowest three electronic states of I_2: the $\widetilde{X}\ ^1\Sigma_g^+$, $\widetilde{A}'\ ^3\Pi_{2u}$, and $\widetilde{A}\ ^3\Pi_{1u}$ states. All three bands exhibit resolved vibrational structure. The band due to the $\widetilde{X}$ state is quite broad, indicating a large geometry change upon photodetachment. Vibrational structure with a typical peak spacing of 0.021 eV is apparent near the center of the band around eKE=0.92 eV, but becomes unresolved at the wings. The $\widetilde{A}$ and $\widetilde{A}'$ bands are considerably narrower. Both bands show resolved vibrational structure with characteristic spacing of 0.011 eV. Although this frequency is considerably lower than in the $\widetilde{X}$ band, the vibrational structure in the $\widetilde{A}'$ and $\widetilde{A}$ bands is well resolved because of their low electron kinetic energy.

The vibrational origin of the $\widetilde{A}$ band is clearly at 0.272 eV; the very weak transitions at higher electron kinetic energy are from hot band transitions originating from vibrationally excited levels of the anion. Since the well depths of all three I_2 states are well known, it is straightforward to assign the somewhat less obvious origin of the $\widetilde{A}'$ band (see Fig. 2) and to assign the vibrational structure in the center of the $\widetilde{X}$ band to transitions to highly excited vibrational levels of I_2. The vibrational structure and assignments are discussed in more detail in Sec. IV B.

B. Femtosecond photoelectron spectroscopy

Figure 3 shows successive femtosecond photoelectron spectra starting at a pump–probe delay of 500 fs and stepping every 25 fs up to 1500 fs. Note that I_2^- can be detached by the probe pulse; this background signal from the probe pulse alone has been subtracted from the spectra in Fig. 3. As shown in our previous work[19] on I_2^-, dissociation to I^-+I is complete by 200 fs, so these spectra at later delay times are dominated by two peaks at 0.77 and 1.70 eV that correspond to transitions from the I^- photo-product to the $^2P_{1/2}$ and $^2P_{3/2}$ states of iodine, respectively. The additional feature of interest in Fig. 3 is the time-varying oscillatory structure su-

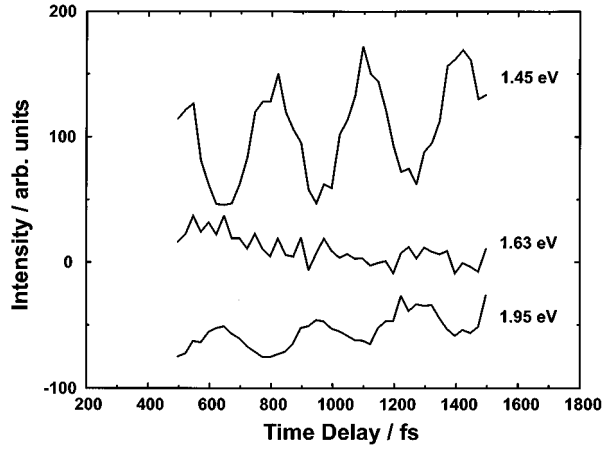

FIG. 4. Slices through FPES spectra of Fig. 3 at 1.45, 1.63, and 1.95 eV.

perimposed on the spectrum. This is most noticeable around eKE=1.45 eV, near the base of the $I(^2P_{3/2})\leftarrow I^-$ transition, but it is apparent over other ranges of electron kinetic energy as well.

The oscillations are seen more clearly in Fig. 4, which shows cuts through the photoelectron spectra at three different electron kinetic energies, 1.45, 1.63, and 1.95 eV. The period of the oscillation at 1.45 and 1.95 eV is approximately 300 fs, but there is a phase shift of 180° between the two data sets. The oscillatory structure is largely absent at 1.63 eV.

Shown in the inset of Fig. 5 is the time slice at 1.45 eV for a much longer experiment, consisting of approximately 30 oscillations over 12 ps. The solid line in Fig. 5 is the Fourier transform of this spectrum; this is dominated by a single frequency at $110\pm2\ \mathrm{cm}^{-1}$.

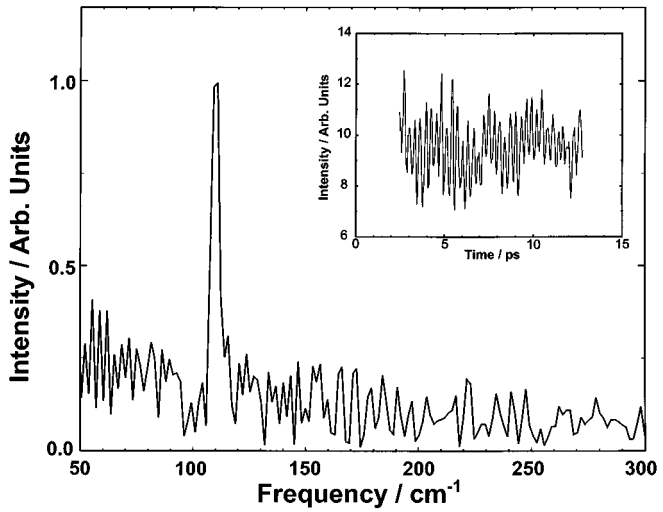

FIG. 5. Solid graph is the Fourier transform at 1.45 eV of long-time FPES experiment, shown in the inset, consisting of 265 spectra stepping every 40 fs from 2000 to 12 580 fs.

IV. ANALYSIS AND DISCUSSION

A. Origin and significance of the coherences

In the FPES experiment, the pump pulse excites I_2^- to the repulsive $\tilde{A}'\ ^2\Pi_{g,1/2}$ state. The photoelectron spectrum obtained by photodetachment with the probe pulse follows the evolution to products on this excited state, but the closed-shell atomic I^- product resulting from dissociation on the $\tilde{A}'\ ^2\Pi_{g,1/2}$ state cannot be the origin of the oscillations in Figs. 3 to 5. However, as mentioned above, the probe pulse does have sufficient energy to photodetach I_2^- from its ground electronic state. This suggests that the oscillatory structure in the photoelectron spectrum is associated with coherent vibrational motion induced by the pump pulse on the ground electronic state of I_2^-.

These vibrational coherences are readily understood in the context of previous femtosecond experiments. It is well known that laser pulses shorter than molecular vibrational periods and resonant with an electronic transition can excite coherences in both the ground and excited electronic states.[26–39] If the upper electronic state is bound, excited state coherences can arise from excitation of a coherent superposition of vibrational levels lying within the laser bandwidth. The concurrent generation of coherences in the ground electronic state is a somewhat more subtle effect, because if one is starting in the ground vibration-electronic state of a molecule, then the observation of ground state oscillations signifies vibrational excitation. This process is due to resonant impulsive stimulated Raman scattering (RISRS), in which resonant Raman scattering from an ultrafast pump pulse induces vibrational excitation into nearby eigenstates.[40–44] The resonance enhancement of this process distinguishes it from the non-resonant ISRS process discussed by Nelson and co-workers.[45,46] The extent to which RISRS occurs and the nature of the resulting wave packet will depend on the pulse energy and bandwidth as well as the shape of the resonant excited state potential. Alternatively, the excitation induced by the pump can be described as ''dynamical hole-burning'' resulting from nonuniform excitation of the initial vibrational wave function.[44,47]

When the RISRS process is active, the probe pulse will typically detect vibrational coherences arising from both the ground and excited states. However, when the excited state is dissociative,[48,49] as was the case in the transient absorption experiments on I_3^- by Ruhman and co-workers,[20] the only modulations attributed to I_3^- arise from a coherent superposition of vibrational levels on its ground electronic state.

Our experiment represents another example of resonant excitation with a dissociative upper state. We therefore attribute the oscillations in our spectra to coherences on the ground electronic state of I_2^- created by the RISRS process. Figure 6 illustrates how a nonstationary wave packet on the ground state results in oscillations in the photoelectron spectrum. As the wave packet evolves, its Franck–Condon overlap with the I_2 vibrational levels changes. Thus, for example, one expects photodetachment to the I_2 ground state when the anion wave packet is at its inner turning point to produce faster electrons than at its outer turning point, because the

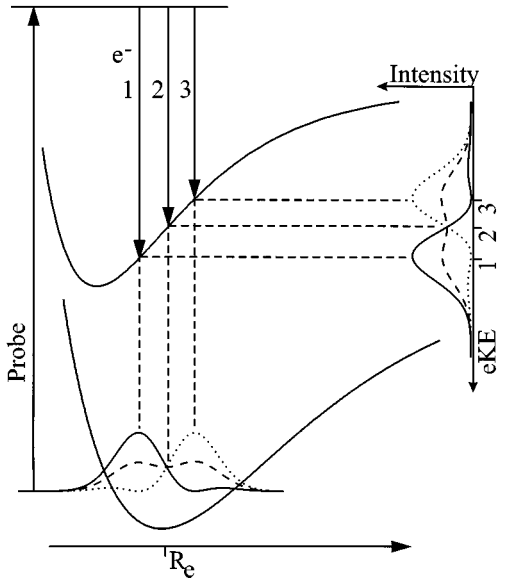

FIG. 6. Effect of wave packet motion on photoelectron spectrum. Time evolution of coherent superposition of $v=0$ and 1 vibrational eigenstates (with equal amplitude) is shown on anion potential at bottom of figure. Photoelectron signal at the three electron kinetic energies indicated are most sensitive to the wave packet intensity at (1) $R<R_e$, (2) $R=R_e$, and (3) $R>R_e$. Right: Photoelectron spectra taken at three delay times corresponding to the three wave functions shown on the anion potential. The signals at energies (1) and (3) are out of phase by 180°, while the signal at (2) remains constant.

vertical detachment energy is less at the inner turning point (compare solid and dotted lines in Fig. 6). This is the origin of the phase shift in the oscillations shown in Fig. 4; electron kinetic energies of 1.45 and 1.95 eV correspond to detachment at internuclear distances larger and smaller than the equilibrium bond length, respectively.

Fourier transforms were taken at 25 meV slices over the entire range of kinetic energies. Each slice is analogous to a single transient absorption experiment with a fixed probe frequency. In each case, the Fourier transform is dominated at most by a single peak, which is most prominent at eKE=1.45 eV as shown in Fig. 5. The frequency of this peak, $110\pm2\ \mathrm{cm}^{-1}$, is the fundamental vibrational frequency in I_2^-; this is the first accurate gas phase measurement of this value, and it is $5\ \mathrm{cm}^{-1}$ lower than the frequency obtained using Raman spectroscopy in a matrix.

As will be shown in the next section, there is some vibrationally excited I_2^- produced in our ion beam, although most of the population is in the $v=0$ level. The peak in the Fourier transform is therefore primarily a result of a coherent superposition of the $v=0$ and 1 levels resulting from vibrational excitation of the $v=0$ level via the RISRS process. (The pump laser linewidth, $140\ \mathrm{cm}^{-1}$, is larger than the $110\ \mathrm{cm}^{-1}$ spacing of these levels.) Coherences between adjacent levels resulting from RISRS excitation of the vibrationally excited levels of the anion are also expected, but the analysis in the next section shows that the anharmonicity $\omega_e x_e$ is only $0.370\ \mathrm{cm}^{-1}$. This means that the v_{0-1} and v_{1-2} frequencies differ by less than a wavenumber, and this small splitting is apparently not detectable in our experiment. Some of the Fourier transforms at eKE<1.45 eV show evidence for a peak at twice the fundamental frequency, as expected for a coherence between vibrational levels differing by two quanta. However, this peak is at best barely above the noise level, so these coherences are either very weak or nonexistent in our experiment.

One final point of interest is that when the wave packet is only composed of adjacent vibrational levels ($v=0$ and 1, $v=1$ and 2, etc.), the probability density as a function of time is approximately constant at the equilibrium bond length (exactly constant for a harmonic oscillator). This is shown explicitly in Fig. 6. As a result, there should be very little oscillatory structure at eKE values that correspond to vertical detachment near the equilibrium bond length. This is the reason for the absence of oscillations in the energy slice at 1.63 eV in Fig. 4.

B. I_2^- ground state potential

In this section a Morse potential for the ground state of I_2^- is constructed by fitting the conventional photoelectron spectrum in Fig. 2 with the harmonic vibrational frequency, ω_e, constrained to equal the fundamental vibrational frequency v_{0-1} determined in the previous section(see below). Since the Morse potential only has three parameters

$$V(r)=D_e[1-e^{-\beta(R-R_e)}]^2, \tag{2}$$

where

$$\beta=\omega_e\left(\frac{2\pi^2\mu}{D_e}\right)^{1/2} \tag{3}$$

and μ is the reduced mass, the analysis in this section is aimed at determining the well depth, D_e, and equilibrium internuclear separation, R_e. This information can be extracted from the photoelectron spectrum in Fig. 2 because (a) the neutral states of I_2 are very well characterized from fluorescence measurements,[15–18] and (b) the origin of the band corresponding to photodetachment to the $\tilde{A}\ ^3\Pi_{1u}$ state of I_2 at $\mathrm{eKE}(\tilde{A})=0.272\pm0.005$ eV can be assigned by inspection.

The adiabatic electron affinity of I_2 is then given by

$$\mathrm{EA}(I_2)=h\nu-\mathrm{eKE}(\tilde{A})-T_0(\tilde{A}), \tag{4}$$

where $T_0(\tilde{A})=1.345$ eV is the electronic term value for the $\tilde{A}\ ^3\Pi_{1u}$ state of I_2.[15] This yields 2.524 ± 0.005 eV for the electron affinity of I_2, in contrast to the previous, averaged literature value of 2.55 eV.[8] The well depth $D_0(I_2^-)$ is then determined from

$$D_0(I_2^-)=\mathrm{EA}(I_2)+D_0(I_2)-\mathrm{EA}(I). \tag{5}$$

Using $D_0(I_2)=1.542$ eV and EA(I)=3.059 eV (Refs. 18 and 50), we find $D_0(I_2^-)=1.007$ eV. The well depth, $D_e=1.014$ eV is determined by adding the anion zero point vibrational energy (assumed to be $\omega_e/2$) of 0.007 eV. The anharmonicity $\omega_e x_e$ can then be from obtained from

$$\omega_e x_e=\frac{\omega_e^2}{4D_e} \tag{6}$$

yielding $\omega_e x_e = 0.370\ \mathrm{cm}^{-1}$. This small value justifies setting $\omega_e = \upsilon_{01}$.

With the well depth and vibrational frequency of I_2^- determined, R_e can be obtained through simulations of the conventional photoelectron spectrum within the Franck–Condon approximation. The discrete variable representation (DVR) with a Morse oscillator basis set[51] was used to calculate anion and neutral vibrational wave functions and the Franck–Condon factors between the anion and the three neutral states. The anion R_e and vibrational populations were varied, and the simulation was convoluted with an instrument response function to accurately reproduce the neutral state vibrational progressions. The final Morse parameters are given in Table I, and the simulated spectrum and assumed vibrational distribution for the I_2^- are shown in Fig. 2.

The effects of hot bands on the spectrum are quite pronounced. Peaks solely due to hot bands are seen on the high electron kinetic energy side of the origin transitions for the $\tilde{A}$ and $\tilde{A}'$ bands. They also add intensity to transitions originating from the $I_2^-(\upsilon=0)$ level. The effects of hot bands can also be seen in the $\tilde{X}$ band. Because of the large geometry change upon photodetachment to the $\tilde{X}$ state, the spatial extent and nodal structure of the anion vibrational wavefunctions are reflected in the intensity profile in the photoelectron spectrum. Thus transitions originating from the $I_2^-(\upsilon=0)$ level have an approximately Gaussian intensity profile, while those from $I_2^-(\upsilon=1)$ have a bimodal intensity profile extending to higher and lower final vibrational levels than the $\upsilon=0$ transitions, but with relatively little intensity at the center of the $\upsilon=0$ profile. The net effect is that vibrational structure is resolved in the center of the $\tilde{X}$ band, as these are primarily transitions from the anion $\upsilon=0$ level, while transitions from multiple anion vibrational levels contribute to the wings of the $\tilde{X}$ band, resulting in overlapped transitions that cannot be resolved by our spectrometer. Although there is some range in the anion population within which the spectrum can be successfully simulated, R_e did not change by more than 0.005 Å over this range.

Table I compares our Morse parameters with four other potentials proposed for the I_2^- ground state: the empirical potentials of Chen and Wentworth,[8] Dojahn *et al.*,[9] and Chen *et al.*,[10] and the *ab initio* potential of Maslen *et al.*[14] The original Chen and Wentworth potential is closest to ours, although our potential well is not as deep (1.014 vs 1.10 eV), and our value for R_e is smaller (3.205 vs 3.23 Å). As an indication of the sensitivity of the photoelectron spectrum to the potential parameters, Fig. 7 shows simulations using the Chen and Wentworth potential (dashed), superimposed on the experimental spectrum (solid). The simulated $\tilde{A}'$ and $\tilde{A}$ bands occur at about 0.1 eV lower eKE than the experimental bands, indicating that the anion potential well is too deep. The even larger shift of 0.2 eV in the center of the simulated $\tilde{X}$ band and the differences in the Franck–Condon profiles for all three bands result from the overly large bond length in the anion potential. Note that the more recent potentials by Dojahn *et al.* and Chen *et al.* are progressively moving away from our parameters, implying that the assumptions made about the bond length and the correlation between the anions and positive ion dimers are not reliable for the case of I_2^-.

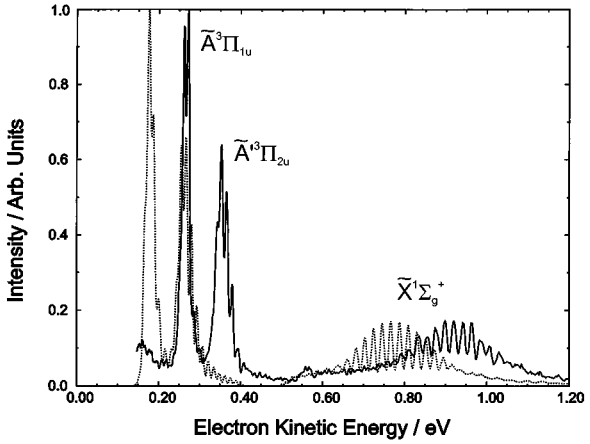

FIG. 7. Experimental (solid) and simulated (dashed) photoelectron spectrum of I_2^- using the Chen and Wentworth potential (Ref. 8).

V. CONCLUSION

The ground state of I_2^- has been fit to a Morse function. The vibrational frequency is obtained from a femtosecond photoelectron spectroscopy experiment, in which resonant impulsive stimulated Raman scattering (RISRS) induced by the pump pulse leads to oscillatory structure in the time-dependent photoelectron spectra. The well depth and equilibrium bond length are derived from a Franck–Condon analysis of the high resolution photoelectron spectrum of I_2^- which consists of vibrationally resolved transitions to the three lowest electronic states of I_2. Our results yield a shallower well depth and a shorter bond length than the previously published semiempirical potentials.

The results presented here show FPES and conventional photoelectron spectroscopy to be a complementary and powerful set of techniques to probe anion potential energy features. The demonstration of the RISRS process on gas-phase anions and the resulting determination of the I_2^- vibrational frequency suggests that the FPES experiment will be useful in measuring vibrational frequencies of other molecular and cluster anions.

ACKNOWLEDGMENTS

This research is supported by the National Science Foundation under Grant No. CHE-9404735. Support from the Defense University Research Instrumentation Program and Air Force Office of Scientific Research under Grant No. F49620-95-1-0078 is also gratefully acknowledged. The authors also thank Robert J. Le Roy for providing the RKR algorithm and Joel Tellinghuisen for insight into the $\tilde{A}'$ neutral state.

[1] J. M. Papanikolas, J. R. Gord, N. E. Levinger, D. Ray, V. Vorsa, and W. C. Lineberger, J. Phys. Chem. **95**, 8028 (1991).
[2] J. M. Papanikolas, V. Vorsa, M. E. Nadal, P. J. Campagnola, H. K. Buchenau, and W. C. Lineberger, J. Chem. Phys. **99**, 8733 (1993).

[3] V. Vorsa, S. Nandi, P. J. Campagnola, M. Larsson, and W. C. Lineberger, J. Chem. Phys. **106**, 1402 (1997).
[4] B. J. Greenblatt, M. T. Zanni, and D. M. Neumark, Science **276**, 1675 (1997).
[5] I. Benjamin, P. F. Barbara, B. J. Gertner, and J. T. Hynes, J. Phys. Chem. **99**, 7557 (1995).
[6] A. E. Johnson, N. E. Levinger, and P. F. Barbara, J. Phys. Chem. **96**, 7841 (1992).
[7] P. K. Walhout, J. C. Alfano, K. A. M. Thakur, and P. F. Barbara, J. Phys. Chem. **99**, 7568 (1995).
[8] E. C. M. Chen and W. E. Wentworth, J. Phys. Chem. **89**, 4099 (1985).
[9] J. G. Dojahn, E. C. M. Chen, and W. E. Wentworth, J. Phys. Chem. **100**, 9649 (1996).
[10] E. C. M. Chen, J. G. Dojahn, and W. E. Wentworth, J. Phys. Chem. A **101**, 3088 (1997).
[11] P. W. Tasker, G. G. Balint-Kurti, and R. N. Dixon, Mol. Phys. **32**, 1651 (1976).
[12] G. A. Bowmaker, P. Schwerdfeger, and L. v. Szentpaly, J. Mol. Struct. Theochem. **53**, 87 (1989).
[13] D. Danonvich, J. Hrusak, and S. Shaik, Chem. Phys. Lett. **233**, 249 (1995).
[14] P. E. Maslen, J. Faeder, and R. Parson, Chem. Phys. Lett. **263**, 63 (1996).
[15] D. R. T. Appadoo, R. J. Leroy, P. F. Bernath, S. Gerstenkorn, P. Luc, J. Verges, J. Sinzelle, J. Chevillard, and Y. Daignaux, J. Chem. Phys. **104**, 903 (1996).
[16] X. N. Zheng, S. L. Fei, M. C. Heaven, and J. Tellinghuisen, J. Chem. Phys. **96**, 4877 (1992).
[17] J. W. Tromp and R. J. Le Roy, J. Mol. Spectrosc. **109**, 352 (1985).
[18] F. Martin, R. Bacis, S. Churassy, and J. Verges, J. Mol. Spectrosc. **116**, 71 (1986).
[19] B. J. Greenblatt, M. T. Zanni, and D. M. Neumark, Chem. Phys. Lett. **258**, 523 (1996).
[20] U. Banin and S. Ruhman, J. Chem. Phys. **98**, 4391 (1993).
[21] C. Xu, G. R. Burton, T. R. Taylor, and D. M. Neumark, J. Chem. Phys. (in press, 1997).
[22] R. B. Metz, A. Weaver, S. E. Bradforth, T. N. Kitsopoulos, and D. M. Neumark, J. Phys. Chem. **94**, 1377 (1990).
[23] R. Prosch and T. Trickl, Rev. Sci. Instrum. **60**, 713 (1989).
[24] W. C. Wiley and I. H. McLaren, Rev. Sci. Instrum. **26**, 1150 (1955).
[25] O. Cheshnovsky, S. H. Yang, C. L. Pettiette, M. J. Craycraft, and R. E. Smalley, Rev. Sci. Instrum. **58**, 2131 (1987).
[26] M. J. Rosker, F. W. Wise, and C. L. Tang, Phys. Rev. Lett. **57**, 321 (1986).
[27] J. M. Y. Ha, H. J. Maris, W. M. Risen, Jr., J. Tauc, C. Thomsen, and Z. Vardeny, Phys. Rev. Lett. **57**, 3302 (1986).
[28] K. A. Nelson and L. R. Williams, Phys. Rev. Lett. **58**, 745 (1987).
[29] B. Hartke, R. Kosloff, and S. Ruhman, Chem. Phys. Lett. **158**, 238 (1989).
[30] R. M. Bowman, M. Dantus, and A. H. Zewail, Chem. Phys. Lett. **161**, 297 (1989).
[31] M. Gruebele, G. Roberts, M. Dantus, R. M. Bowman, and A. H. Zewail, Chem. Phys. Lett. **166**, 459 (1990).
[32] T. Baumert, V. Engel, C. Meier, and G. Gerber, Chem. Phys. Lett. **200**, 488 (1992).
[33] S. Rutz, S. Greschik, E. Schreiber, and L. Woste, Chem. Phys. Lett. **200**, 488 (1992).
[34] T. Baumert, V. Engel, C. Rottgermann, W. T. Strunz, and G. Gerber, Chem. Phys. Lett. **191**, 639 (1992).
[35] M. Gruebele and A. H. Zewail, J. Chem. Phys. **98**, 883 (1993).
[36] G. Rodriguez and J. G. Eden, Chem. Phys. Lett. **205**, 371 (1993).
[37] H. Ruppe, S. Rutz, E. Schrieber, and L. Woste, Chem. Phys. Lett. **257**, 356 (1996).
[38] R. de Vivie-Riedle, K. Kobe, J. Manz, W. Meyer, B. Reischl, S. Rutz, E. Schreiber, and L. Woste, J. Phys. Chem. **100**, 7789 (1996).
[39] A. Assion, M. Geisler, J. Helbing, V. Seyfried, and T. Baumert, Phys. Rev. A **54**, R4605 (1996).
[40] A. Mokhtari and J. Chesnoy, Europhys. Lett. **5**, 523 (1988).
[41] J. Chesnoy and A. Mokhtari, Phys. Rev. A **38**, 3566 (1988).
[42] S. L. Dexheimer, Q. Wang, L. A. Peteanu, W. T. Pollard, R. A. Mathies, and C. V. Shank, Chem. Phys. Lett. **188**, 61 (1992).
[43] W. T. Pollard and R. A. Mathies, Annu. Rev. Phys. Chem. **43**, 497 (1992).
[44] U. Banin, A. Bartana, S. Ruhman, and R. Kosloff, J. Chem. Phys. **101**, 8461 (1994).
[45] S. de Silvestri, J. G. Fujimoto, E. P. Ippen, E. B. Gamble, Jr., L. R. Williams, and K. A. Nelson, Chem. Phys. Lett. **116**, 146 (1985).
[46] Y. Yong-Xin, E. B. Gamble, Jr., and K. A. Nelson, J. Chem. Phys. **83**, 5391 (1985).
[47] D. M. Jonas, S. E. Bradforth, S. A. Passino, and G. R. Fleming, J. Phys. Chem. **99**, 2594 (1995).
[48] N. F. Scherer, L. D. Ziegler, and G. R. Fleming, J. Chem. Phys. **97**, 5544 (1992).
[49] N. F. Scherer, D. M. Jonas, and G. R. Fleming, J. Chem. Phys. **99**, 153 (1993).
[50] H. Hotop and W. C. Lineberger, J. Phys. Chem. Ref. Data **14**, 731 (1985).
[51] E. M. Greenawalt and A. S. Dickinson, J. Mol. Spectrosc. **30**, 427 (1969).